Smoothed Finite Element Methods for Nonlinear Solid Mechanics Problems: 2D and 3D Case Studies

Manfred Staat [1] and **Minh Tuấn Dương** [2]

[1] *Faculty of Medical Engineering and Applied Mathematics, FH Aachen University of Applied Sciences, Campus Jülich, Heinrich-Mußmann-Str. 1, 52428 Jülich, Germany*
Email: m.staat@fh-aachen.de
[2] *School of Mechanical Engineering, Hanoi University of Science and Technology, No. 1 Dai Co Viet Road, Hanoi, Vietnam.*
Email: tuan.duongminh@hust.edu.vn

Abstract: The Smoothed Finite Element Method (SFEM) is presented as an edge-based and a face-based techniques for 2D and 3D boundary value problems, respectively. SFEMs avoid shortcomings of the standard Finite Element Method (FEM) with lower order elements such as overly stiff behavior, poor stress solution, and locking effects. Based on the idea of averaging spatially the standard strain field of the FEM over so-called smoothing domains SFEM calculates the stiffness matrix for the same number of degrees of freedom (DOFs) as those of the FEM. However, the SFEMs significantly improve accuracy and convergence even for distorted meshes and/or nearly incompressible materials. Numerical results of the SFEMs for a cardiac tissue membrane (thin plate inflation) and an artery (tension of 3D tube) show clearly their advantageous properties in improving accuracy particularly for the distorted meshes and avoiding shear locking effects.

Keywords: *SFEM, ES-FEM, FS-FEM, FEM, hyperelastic materials and nonlinear analysis.*

1. Introduction

The Finite Element Method (FEM) has been developed for over a half of a century. Developments of lower-order elements, which are widely used in engineering applications, were remarkable [1, 2]. We are interested in two/three-dimensional (2D/3D) nonlinear solid problems solved by the FEM using 3-node triangular elements (FEM-T3) and the FEM with 4-node tetrahedral elements (FEM-T4) since they can automatically be created for any geometry, however complicated, such as machine parts and human organs. Nevertheless, these elements face crucial shortcomings such as the well-known overly stiff behavior, poor stress solution, and locking effects. Thus multifield variational problems have been proposed to overcome these disadvantages.

Inspired by the work of Chen et al. [3] on stabilized conforming nodal integration, Liu et al. [4] introduced the Smoothed Finite Element Method (SFEM). The principal idea of SFEM is to formulate a strain field as a spatial average of the standard strain measure. To this end, the elements are divided into smoothing domains (or smoothing cells) over which the strain is smoothed. The smoothing domains are associated with the boundary of two neighboring elements. Specifically, four different smoothing domains created based on cells (elements), nodes, edges, and faces are used to establish four different formulations of the SFEM: cell-based SFEM (CS-FEM), node-based SFEM (NS-FEM), edge-based SFEM (ES-FEM), and face-based SFEM (FS-FEM) [5]. Each of the four variants of SFEM has different advantages and disadvantages [5]. The ES-FEM has been adopted for nonlinear problem [6]. In biomechanics or biomedical engineering, there are very few studies using the SFEM [6, 7]. SFEM combined with the extended FEM (XFEM) can avoid the singularity at the crack tip of the discontinuity of the model [8]. Herein, the ES-FEM-T3 and the FS-FEM-T4 are presented in detail for nonlinear solid mechanics problems arising from metal forming, deep forming, etc. A number of numerical results is presented to exhibit the efficiency and advantageous properties of the two models.

2. Smoothed Finite Element Formulations

In this section, the two smoothed finite elements models are presented using the total Lagrangian formulation.

2.1. Edge-based Smoothed Finite Element Formulation (ES-FEM)

In general, one can apply the ES-FEM to a 2D mesh with polygonal elements and T3 elements as depicted in Fig. 1. However, this section is mainly focused on the basis of the ES-FEM using T3 elements, and the smoothing domain creation [5] is similar to the one in Fig. 1. Moreover, variational details and proofs of the ES-FEM are omitted since they can be found in Liu and Nguyen [5].

A 2D domain Ω is discretized with n_e triangular elements (T3) and n_n nodes such that $\Omega = \cup_{m=1}^{n_e} \Omega_m^e$ and $\Omega_i^e \cap \Omega_j^e = \Theta, \quad i \neq j$. The T3 mesh shall have a total of n_{eg} edges. The virtual displacements $\boldsymbol{u}^h(\boldsymbol{x})$, and the compatible strains $\boldsymbol{\varepsilon}^h(\boldsymbol{x}) = \nabla_s \boldsymbol{u}$ (∇_s is the symmetric part of displacement gradient) within any element can be computed as

$$\boldsymbol{u}^h(\boldsymbol{x}) = \sum_I^{n_d} \boldsymbol{N}_I \boldsymbol{u}_I = \boldsymbol{N}_I \boldsymbol{u}_I, \tag{1}$$

$$\boldsymbol{\varepsilon}^h(\boldsymbol{x}) = \sum_I^{n_d} \boldsymbol{B}_I \boldsymbol{u}_I = \boldsymbol{B}_I \boldsymbol{u}_I \tag{2}$$

where $\boldsymbol{N}$ is the vector of the shape functions used to interpolate the strain, displacement and stress fields; $\boldsymbol{B}$ is the strain-displacement matrix.

a. Smoothing Domain Generation

The smoothing domain (SD) Ω^k is associated with the edge k of the elements, and hence, the number of smoothing domains $n_s = n_{eg}$ (the number of edges). The edge-based smoothing domain is created by connecting two endpoints of the edge to the barycenters of the adjacent elements as illustrated in Fig. 2. In this case, the SD Ω^k consists of n_{sb}^k subsmoothing domains Ω_q^k each of which is a part of the elements concerning the SD Ω^k. Thus, n_{sb}^k is in fact the number of elements sharing the common edge k. The edge divides Ω^k into subsmoothing domains Ω_q^k, $q = 1, 2, ..., n_{sb}^k$, and hence, also forms the interfaces between these Ω_q^k. For an inner edge (at least one of these two ending nodes of the edge located inside the domain) $n_{sb}^k = 2$, and for a boundary edge m (both ending nodes of the edge are located on the boundary Γ_{sb}^k) $n_{sb}^k = 1$.

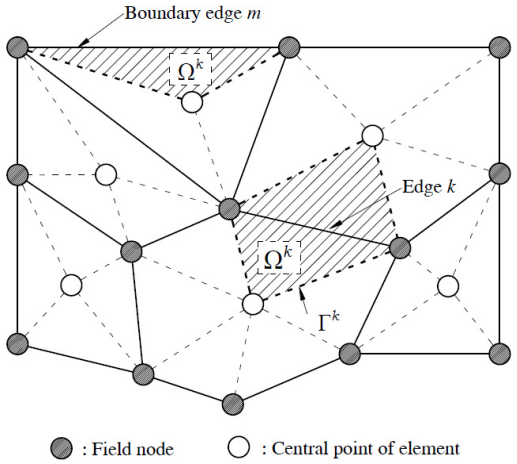

Fig 1. 2D Smoothing domain creation.

All kinds of S-FEM share the idea of smoothing the strain over smoothing domains Ω_i^k as

$$\bar{\boldsymbol{\varepsilon}}_i = \bar{\boldsymbol{\varepsilon}}_i(\boldsymbol{x}_i) = \int_{\Omega_i^k} W(\boldsymbol{x}_i - \boldsymbol{x}) \boldsymbol{\varepsilon}(\boldsymbol{x}) d\Omega \tag{3}$$

with $\boldsymbol{\varepsilon}(\boldsymbol{x})$ being the usual (compatible) strain, W representing a scalar weight function and $\bar{\boldsymbol{\varepsilon}}_i$ being the smoothed strain in Ω_i^k. Usually W is chosen in the way such that the smoothed strain becomes an area-weighted average of the strain. In the SD W reads as

$$W(\boldsymbol{x}_i - \boldsymbol{x}) = \begin{cases} \dfrac{1}{A_i^k}, & \boldsymbol{x} \in \Omega_i^k \\ 0, & \boldsymbol{x} \notin \Omega_i^k \end{cases}, \tag{4}$$

with A_i^k the area of the i^{th} subsmoothing domain. For each part of the total strain $\bar{\boldsymbol{\varepsilon}}_i$ for example linear part and the nonlinear part of the strain are

$$\bar{\boldsymbol{\varepsilon}}_i^l = \frac{1}{A_i^s} \int_{\Omega_i^s} \boldsymbol{\varepsilon}_i^l(\mathbf{x}) d\Omega, \quad \bar{\boldsymbol{\varepsilon}}_i^{nl} = \frac{1}{A_i^s} \int_{\Omega_i^s} \boldsymbol{\varepsilon}_i^{nl}(\mathbf{x}) d\Omega, \tag{5}$$

where $\bar{\boldsymbol{\varepsilon}}_i^l$, $\bar{\boldsymbol{\varepsilon}}_i^{nl}$ are the smoothed linear and nonlinear strain parts of the subsmoothing domain, respectively. By means of the smoothing function, the total strain is smoothed. Alternatively, the strain can be smoothed by performing averaging procedure a standard FE computation. Herein, the general way to derive the smoothed strain field is to use the differential operator $\boldsymbol{L}_d$

$$\bar{\boldsymbol{\varepsilon}}_i^l(\boldsymbol{x}_i) = \int_{\Omega_i^k} \boldsymbol{L}_d \bar{\boldsymbol{u}}(\boldsymbol{x}) W(\boldsymbol{x}_\perp - \boldsymbol{x}) \boldsymbol{\varepsilon}(\boldsymbol{x}) d\Omega \tag{6}$$

Using integration by parts Eq. (6) is written into an integral over the boundary Γ_i^k of the SD

$$\bar{\boldsymbol{\varepsilon}}^{I}(\boldsymbol{x}_i)=\int_{\Gamma_i^s}\boldsymbol{L}_n\bar{\boldsymbol{u}}(\boldsymbol{x})W(\boldsymbol{x}_i-\boldsymbol{x})d\Gamma-\int_{\Omega_i^s}\bar{\boldsymbol{u}}(\boldsymbol{x})\underbrace{\dot{W}(\boldsymbol{x}_i-\boldsymbol{x})}_{=0}d\Omega=\frac{1}{A_i^k}\int_{\Gamma_i^k}\underbrace{\begin{bmatrix}n_1&0\\0&n_2\\n_2&n_1\end{bmatrix}}_{\boldsymbol{L}_n}\bar{\boldsymbol{u}}(\boldsymbol{x})d\Gamma\ \forall\boldsymbol{x}\in\Omega_i^k. \quad (7)$$

It is apparent that $\boldsymbol{L}_n$ contains the components of the outward normal vector on the boundary of the SD. Since the SDs are created based on the edges of the FE mesh the following local computations are hence performed on each SD instead of each element. Besides, the local quantities now lie on SDs the discretization of Eq. (5) becomes as

$$\bar{\boldsymbol{\varepsilon}}_i^{I}(\boldsymbol{x}_i)=\sum_{I}^{N_n}\bar{\boldsymbol{B}}_I^{I}(\boldsymbol{x}_i)\boldsymbol{d}_I \quad (8)$$

with N_n being the number of nodes related to the SD Ω^k, $\bar{\boldsymbol{B}}_i^I$ being the respective smoothed strain-displacement matrix and $\boldsymbol{d}_I$ being the nodal displacement at node I. It is worth noting that the computation of the global smoothed displacement field needs the standard nodal shape functions $\boldsymbol{N}_I$ to form

$$\bar{\boldsymbol{u}}(\boldsymbol{x})=\sum_{I}^{N}\boldsymbol{N}_I(\boldsymbol{x})\bar{\boldsymbol{d}}_I \quad (9)$$

where n_n is the total number of nodes in the FE mesh. From Eqs.(7), (8) and (9) it is now possible to construct

$$\bar{\boldsymbol{B}}_i^I=\frac{1}{A_i^k}\int_{\Gamma_i^k}\boldsymbol{L}_n(\boldsymbol{x})\boldsymbol{N}_I(\boldsymbol{x})d\Gamma=\begin{bmatrix}\bar{b}_{I1}&0\\0&\bar{b}_{I2}\\\bar{b}_{I2}&\bar{b}_{I1}\end{bmatrix} \quad (10)$$

with $\bar{\boldsymbol{b}}_I(\boldsymbol{x}_i)=\frac{1}{A_i^k}\int_{\Gamma_i^k}\boldsymbol{N}_I(\boldsymbol{x})\boldsymbol{n}_i(\boldsymbol{x})d\Gamma.$

By placing Gauss points in the center of each boundary segment of the smoothing domain (e.g. Γ_i^k) the $\bar{\boldsymbol{b}}_I(\boldsymbol{x}_i)$ is calculated as

$$\bar{\boldsymbol{b}}_I(\boldsymbol{x}_i)=\frac{1}{A_i^k}\sum_{k=1}^{n_s}\boldsymbol{N}_I(\boldsymbol{x}_k^{GP})\boldsymbol{n}_i(\boldsymbol{x}_k^{GP})l_k \quad (11)$$

with n_s being the number of boundary segments, $\boldsymbol{x}_k^{GP}$ - the Gauss point at the centre of segment Γ_i^k, $\boldsymbol{n}_i$ - the outward normal vector and l_k - the length of segment Γ_i^k.

b. Discrete Shear Gap Method

It is well-known that when low order plate elements are utilized in the FEM for nonlinear 3D problems, the transverse shear locking will occur to cause a large error in the solution. To apply the ES-FEM to a plate inflation test, the Discrete Shear Gap (DSG) method is utilized to avoid transverse shear locking. The respective formulae are given in Cui *et al.* [9]. We introduce the element coordinate system ξ_1 and ξ_2 as well as the smoothing coordinate system $\bar{\xi}^1$ as shown in Fig. 2.

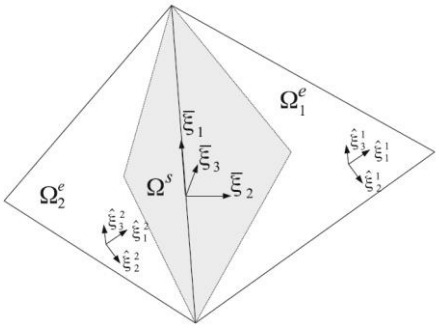

Fig 2. Element and SD coordinate systems [6].

The global smoothed tangent stiffness matrix in the SD coordinate system is then given by

$$\bar{\boldsymbol{K}}_{IJ}^t=\sum_{i=1}^{N_s}\left(\bar{\boldsymbol{B}}_i\right)_I^T\boldsymbol{D}\left(\bar{\boldsymbol{B}}_i\right)_J A_i+\sum_{i=1}^{N_s}\left(\bar{\boldsymbol{G}}_i\right)_I^T\boldsymbol{N}\left(\bar{\boldsymbol{G}}_i\right)_J A_i, \quad (12)$$

with N_s the number of smoothing domains,

$$\left(\bar{\boldsymbol{G}}_i\right)_I=\begin{bmatrix}0&0&\bar{b}_{I1}&0&0\\0&0&\bar{b}_{I2}&0&0\end{bmatrix},\ \boldsymbol{N}=\begin{bmatrix}N_{11}&N_{12}\\N_{21}&N_{22}\end{bmatrix} \quad (13)$$

$\boldsymbol{N}$ the matrix of membrane stress resultants.

2.2. Face-based Smoothed Finite Element Method (FS-FEM)

Based on the common faces of elements, the smoothing strain technique [5] is applied to create smoothing domains, such that $\Omega=\cup_{m=1}^{n_f}\Omega_m^k$ and $\Omega_i^k\cap\Omega_j^k=\varnothing$, $i\neq j$ (n_f the number of faces used to create smoothing domains of the whole domain). The smoothing domain Ω^k associated with the face k is formed by simply connecting three nodes of the face to the centers of the adjacent elements as depicted in Fig. 3. Similarity to the ES-FEM smoothing domain generation, W is chosen in the way such that the smoothed strain becomes an volume-weighted average of the strain reads as

$$W(\boldsymbol{x}_i-\boldsymbol{x})=\begin{cases}\frac{1}{V_i^k}, & \boldsymbol{x}\in\Omega_i^k\\0, & \boldsymbol{x}\notin\Omega_i^k\end{cases} \quad (14)$$

with V_i^k the volume of the i^{th} subsmoothing domain. Consequently, the smoothed strain

matrix can generally be evaluated on the smoothing domain Ω_i^k as

$$\bar{\boldsymbol{B}}_i^l = \frac{1}{V_i^k}\int_{\Omega_i^k} \boldsymbol{L}_n(\boldsymbol{x})\phi_l(\boldsymbol{x})dV = \begin{bmatrix} \bar{b}_{l1} & 0 & 0 \\ 0 & \bar{b}_{l2} & 0 \\ 0 & 0 & \bar{b}_{l3} \\ \bar{b}_{l2} & \bar{b}_{l1} & 0 \\ 0 & \bar{b}_{l3} & \bar{b}_{l2} \\ \bar{b}_{l3} & 0 & \bar{b}_{l1} \end{bmatrix} \quad (15)$$

The nonlinear part $\bar{\boldsymbol{B}}_i^{nl}$ of the total $\bar{\boldsymbol{B}}(\boldsymbol{x}_k)$ is similarly smoothed as the linear part $\bar{\boldsymbol{B}}_i^l$. The alternative approach is to smooth the deformation gradient tensor $\bar{\boldsymbol{F}}^k(\boldsymbol{x})$. $\bar{\boldsymbol{F}}^k(\boldsymbol{x})$ is obtained over the SD V^k by the divergence theorem as

$$\bar{\boldsymbol{F}}^k(\boldsymbol{x}) = \frac{1}{V^k}\int_{V^k}\frac{\partial \boldsymbol{u}}{\partial \boldsymbol{X}}dV + \boldsymbol{I} = \bar{\boldsymbol{B}}(\boldsymbol{x}_k)\boldsymbol{u} + \boldsymbol{I}. \quad (16)$$

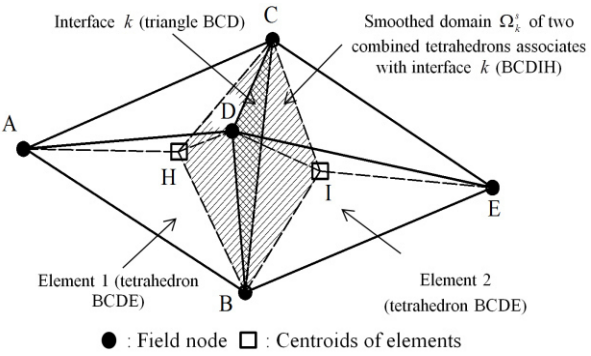

Fig 3. 3D Smoothing domain creation.

2.3. Total Lagrangian Formulation

In this section, the total Lagrangian formulation for the ES-FEM based on the standard FEM. Consider a body, which is subjected to a body force $\boldsymbol{b}_0$ on the reference configuration Ω_0 and the external traction $\boldsymbol{T}$ on the boundary Γ_0. Using the general variational equation in the nonlinear FEM the total virtual work can be evaluated as

$$\delta\Pi(\boldsymbol{u},\delta\boldsymbol{u}) = \delta\boldsymbol{u}^T\int_{\Omega_0}\boldsymbol{B}^T\mathbf{S}dV - \\ -\int_{\Omega_0}\boldsymbol{N}^T\boldsymbol{b}_0dV - \int_{\Gamma_0}\boldsymbol{N}^T\boldsymbol{T}dS = 0. \quad (17)$$

By invoking the arbitrariness of virtual nodal displacements and using load increments with a load factor λ, the FEM formulation and the discrete system of equations can be expressed as

$$\boldsymbol{K}_t\Delta\boldsymbol{u} = (\boldsymbol{K}_M + \boldsymbol{K}_G)\Delta\boldsymbol{u} = \boldsymbol{F}_{\text{int}}(\boldsymbol{u}) - \lambda\boldsymbol{F}_{\text{ext}}(\boldsymbol{u}), \quad (18)$$

where the internal force vector and the external force vector are respectively estimated as

$$\boldsymbol{F}_{\text{int}}(\boldsymbol{u}) = \int_{\Omega_0}\boldsymbol{B}^T\mathbf{S}dV, \\ \boldsymbol{F}_{\text{ext}}(\boldsymbol{u}) = \int_{\Omega_0}\boldsymbol{N}^T\boldsymbol{b}_0dV - \int_{\Gamma_0}\boldsymbol{N}^T\boldsymbol{T}dS. \quad (19)$$

Based on the formulation of the FEM above, the ES-FEM can be achieved. Substituting the total smoothed $\bar{\boldsymbol{B}}$ into Eq. (19) and performing the assembly procedure on the SDs, the smoothed material stiffness matrix for the linearized portion can therefore be estimated as

$$\bar{\boldsymbol{K}}_M = \sum_{k=1}^{n_{eg}}\bar{\boldsymbol{K}}_M^k. \quad (20)$$

The SD tangent stiffness is calculates as

$$\bar{\boldsymbol{K}}_M^k = \int_{\Omega^k}\left(\bar{\boldsymbol{B}}_M^k\right)^T\boldsymbol{D}\bar{\boldsymbol{B}}_M^k dA = \left(\bar{\boldsymbol{B}}_M^k\right)^T\boldsymbol{D}\bar{\boldsymbol{B}}_M^k A^k \quad (21)$$

with $\bar{\boldsymbol{K}}_M^k$ being the smoothed material stiffness on the SD Ω^k with its area A^k associated with the edge k, and $\boldsymbol{D}$ being the constitutive matrix. The second term on the left hand side in Eq. (18) is the geometric stiffness matrix concerning the nonlinearity of $\bar{\boldsymbol{B}}$ and is evaluated as

$$\boldsymbol{K}_G = \sum_{k=1}^{n_{eg}}\bar{\boldsymbol{K}}_G^k, \quad \bar{\boldsymbol{K}}_G^k = \sum_{k=1}^{n_{eg}}\left(\bar{\boldsymbol{B}}_G^k\right)^T\bar{\boldsymbol{S}}_G\bar{\boldsymbol{B}}_G^k A^k, \quad (22)$$

where $\bar{\boldsymbol{S}}_G$ is obtained by smoothing the $\boldsymbol{S}_G$ of the element, see [7], is the hyper-diagonal matrix of the second Piola-Kirchhoff stress. The internal force vector is now calculated based on the stress on the SD, represented as

$$\boldsymbol{F}_{\text{int}}(\boldsymbol{u}) = \int_{\Omega_0}\bar{\boldsymbol{B}}^T\bar{\mathbf{S}}dV = \sum_{k=1}^{n_{eg}}\left(\bar{\boldsymbol{B}}^k\right)^T\bar{\mathbf{S}}A^k \quad (23)$$

The remaining calculations are similar to those of the 3D case using the FS-FEM-T4, see [7]. One can base on the above formulae for 2D cases and replace n_{eg} and A^k by n_f and V^k, respectively.

3. Numerical Results

In this section, numerical results of the ES-FEM and the FS-FEM applied to solid mechanics problems are presented. The advantageous properties of the ES-FEM and the FS-FEM can be found in [5]. Herein, we apply the two SFEM models to our applications with nonlinear material models subjected to large deformations.

a. Inflation of a plate

An experimental setup so-called CellDrum [10] with a membrane of soft tissue is inflated by a pressure. The membrane diameter is 16 *mm* with thickness of 0.008 *mm*. The neo-Hookean model was employed $W = 0.5\mu(I_1 - 3), \quad \mu = 0.166$ kPa.

Due to the symmetry of the problem, only a quarter of the membrane was simulated with the boundary conditions, see Fig. 4. The ES-FEM was then utilized to validate the simulations with the experiments. The numerical results were compared with seven experimental data sets as illustrated in Fig. 5. There is good agreement between the experimental and the numerical pressure-deflection curves [11]. Therefore, the simulation can be used to predict the behavior of the experiments of cardiac tissue construct in the CellDrum [11].

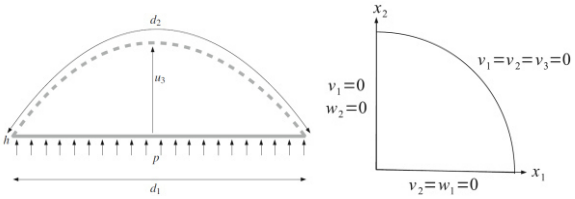

Fig 4. Boundary conditions of a circular plate.

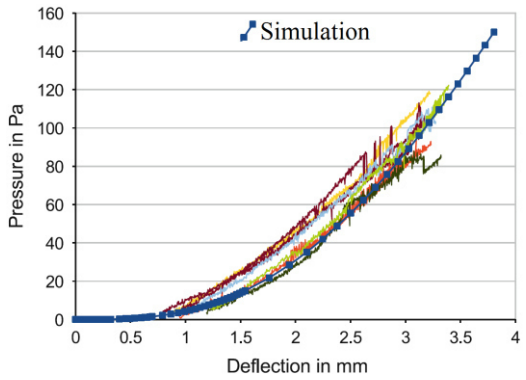

Fig 5. Comparison with seven experimental.

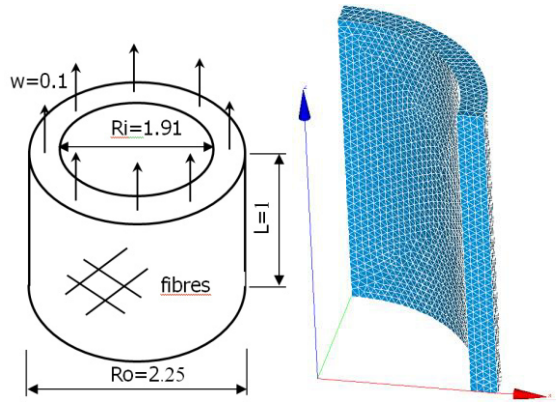

Fig 6. Boundary conditions in uniaxial tests.

b. Uniaxial tension test of artery sample

The artery is an important part of human body in which the blood is flowing und periodic internal pressure. Therefore, it is stretched in hoop direction as well as along the longitudinal direction and hence the length might be extended periodically. To simulate the artery with a similar working condition, a uniaxial tension test can be employed. Moreover, a material law can be tested in order to achieve stable FEM simulations. It means that the material model must result in a physical response as discussed in [12]. The FS-FEM was used to simulate an artery sample subjected to uniaxial tension test, see Fig. 6. A displacement of 0.1 *mm* was prescribed along the longitudinal direction of a quarter of the tube. The material used is the modified Holzapfel model-Model 6 with the parameters in [7]. The numerical results of model 6 are correct since the model behaves physically with the thickness decreasing as expected, see [12], whereas the Holzapfel (HSF) strain-energy function shows non-physical responses as illustrated in Figs. 7 and 8.

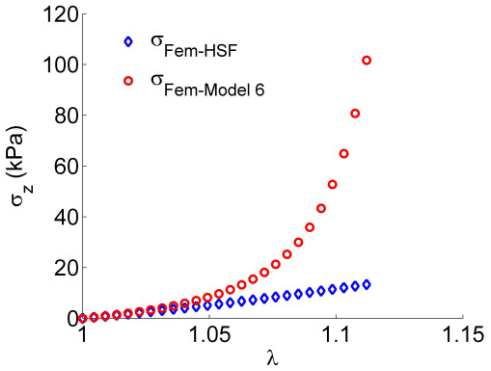

Fig 7. Stress responses of model 6 compared with HSF model in tube tests.

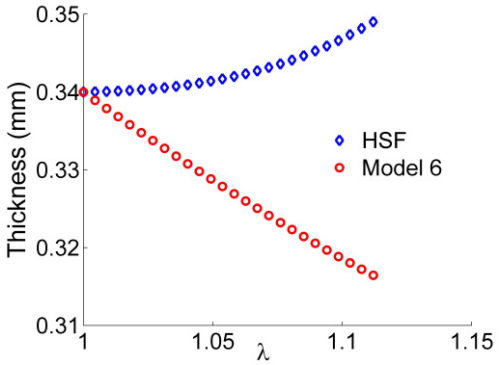

Fig 8. Physical thickness responses of model 6 compared with HSF model in tube tests.

c. Deflection of a beam

The FS-FEM can overcome distorted meshes in a beam (neo-Hookean model, $\mu = 20.273$ kPa) subjected a distributed load as depicted in Fig. 9. The deflection of the tip was adopted for comparisons between the SFEM and the FEM. To this end several FEM models were employed. However, the FS-FEM-T4 for distorted mesh (aspect ratio =22) results in a deflection close to FEM-T4 for non-distorted mesh, indicating an advantageous property, see Fig. 10.

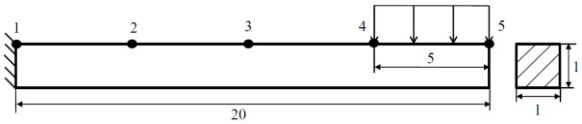

Fig 9. A Beam 20x1x1 [mm^3].

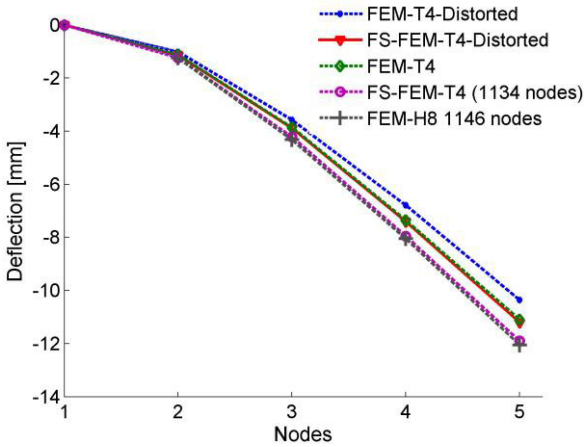

Fig 10. Result comparison between the distorted and non-distorted meshes.

4. Discussion

For the above physically and geometrically nonlinear problems the ES-FEM and the FS-FEM exhibit significantly improved accuracy of the simulation results, particularly for distorted meshes [5]. This is due to the fact that no derivatives of shape functions and no isoparametric mapping in the SFEM are needed. The FS-FEM-T4 is equivalent the FEM-H8 (8-node hexahedral element) due to the interpolating procedure of the both models employing similar number of nodes, leading to a similar estimated strain-displacement matrix. Nevertheless, the SFEM can be immune from locking effect as indicated in the inflated plate. For the tube test there might be a volumetric locking, but this can be solved if the FS-FEM is combined with the NS-FEM. In the tube test the incompressibility condition was imposed with the Poisson ratio $\nu = 0.49$ and an acceptable accuracy can be achieved. Thus, the FS-FEM can be directly applied to nearly incompressible materials with acceptable accuacy.

5. Conclusions

Using the smoothed strain, the overall tangent stiffness of the SFEM obtained is softer, leading to larger deformations. Moreover, no additional DOFs are required to formulate the SFEM.

Consequently, the ES-FEM and FS-FEM shows promising capabilities with significantly improved accuracy and convergence rate even under incompressibility conditions. The outlook is to develop the NS-FEM combined with the FS-FEM using higher order elements for problems incompressible deformations in biomechanics of soft tissues and solid mechanics such as plastic flows in deep forming. More applications using the SFEM for coupled two-phase problems are considered worth to be developed.

6. References

[1] Taylor, R L (2000), A mixed-enhanced formulation tetrahedral finite elements, Int. J. Numer. Methods Eng., vol. 47, no. 1–3, pp. 205–227.

[2] Bonet, J et al (2001), An averaged nodal deformation gradient linear tetrahedral element for large strain explicit dynamic applications, Commun. Numer. Meth. Engng, vol. 17, pp. 551–561.

[3] Chen, J S et al (2001), A stabilized conforming nodal integration for Galerkin mesh-free methods, Int. J. Numer. Meth. Engng, vol. 50, pp. 435–466.

[4] Liu, G. R. et al (2007), A Smoothed Finite Element Method for mechanics problems," Comput. Mech., vol. 39, no. 6, pp. 859–877.

[5] Liu, G R and Nguyen, T T (2010), Smoothed finite element methods. CRC Press, Boca Raton.

[6] Frotscher, R et al (2015), Simulation of cardiac cell-seeded membranes using the edge-based smoothed FEM, Adv. Struct. Mater., vol. 45, pp. 187–212.

[7] Duong, M T (2014), Hyperelastic Modeling and Soft-Tissue Growth Integrated with the Smoothed Finite Element Method-SFEM, PhD Thesis, RWTH Aachen University, Germany.

[8] Bordas, S et al (2010), Strain smoothing in FEM and XFEM, Comput. Struct., vol. 88, no. 23–24, pp. 1419–1443.

[9] Cui, X et al (2009), Analysis of plates and shells using an edge-based smoothed finite element method, Comput. Mech., vol. 45, no. 2, pp. 141–156.

[10] Duong, M T et al (2016), 3D electromechanical FEM-based model for cardiac tissue, in ECCOMAS.

[11] Frotscher, R (2016), Electromechanical modeling and simulation of thin cardiac tissue constructs: smoothed FEM applied to an biomechanical plate problem, PhD Thesis, University of Duisburg-Essen.

[12] Duong, M T et al (2015), Physical response of hyperelastic models for composite materials and soft tissues, Asia Pacific J. Comput. Eng., vol. 2, no. 1, pp. 1–18.